

Article

Kinetic Modelling of Powder-Pack Boronized 4Cr5MoSiV1 Steel by Two Distinct Approaches

Katia Benyakoub ¹, Mourad Keddam ¹ , Brahim Boumaali ¹ and Michał Kulka ^{2,*} 

¹ Laboratoire de Technologie des Matériaux, Faculté G.M. et G.P., USTHB, B.P. No. 32, El-Alia, Bab-Ezzouar, Algiers 16111, Algeria; benyakoub.katia@gmail.com (K.B.); keddam@yahoo.fr (M.K.); brahimboumaali@yahoo.com (B.B.)

² Institute of Materials Science and Engineering, Poznan University of Technology, Pl. M. Skłodowskiej-Curie 5, 60-965 Poznan, Poland

* Correspondence: michal.kulka@put.poznan.pl

Abstract: This work attempts to model the powder-pack boronizing kinetics of 4Cr5MoSiV1 steel in the interval of 1133 and 1253 K in order to predict the layers' thicknesses. The first approach is referred to as the bilayer model and relies on the conservation principle of mass balance equations at the two phase fronts accounting for the linearity of boron distribution across each boride phase. The second approach deals with the application of dimensional analysis to simulate the boronizing kinetics of 4Cr5MoSiV1 steel. Using the bilayer model and the classical parabolic law, the boron activation energies in FeB and Fe₂B were evaluated and discussed in light of the literature data. The estimated boron activation energies from the bilayer model were respectively equal to 164.92 and 153.39 kJ mol⁻¹. These values were very comparable to those calculated from the classical parabolic law. Finally, it was proven that the dimensional analysis was able to simulate the layers' thicknesses for the selected processing parameters.

Keywords: boronizing; iron borides; diffusion; bilayer model; dimensional analysis; activation energy



Citation: Benyakoub, K.; Keddam, M.; Boumaali, B.; Kulka, M. Kinetic Modelling of Powder-Pack Boronized 4Cr5MoSiV1 Steel by Two Distinct Approaches. *Coatings* **2023**, *13*, 1132. <https://doi.org/10.3390/coatings13061132>

Academic Editor: Liqiang Wang

Received: 1 June 2023

Revised: 15 June 2023

Accepted: 16 June 2023

Published: 20 June 2023



Copyright: © 2023 by the authors. Licensee MDPI, Basel, Switzerland. This article is an open access article distributed under the terms and conditions of the Creative Commons Attribution (CC BY) license (<https://creativecommons.org/licenses/by/4.0/>).

1. Introduction

The surface hardening of steels by boronizing is of primary significance to obtain outstanding surface properties. The boronizing treatment is a process in which the release of active boron from any boron source (such as boron carbide, borax, amorphous boron, or boron trichloride) permits its diffusion into the steel's substrate to form a boride layer over its surface via thermal energy [1,2].

The boronizing treatment results in the improvement of the following properties: a high surface hardness of about 1800–2000 HV, resistance to wear [3], and the capability of resistance in acidic and alkaline environments [4,5], as well as in the aggressive liquid solder alloy [6]. The boron element, despite its small size, has a manifest potential to improve the surface hardness of ferrous and non-ferrous alloys (i.e., titanium alloys and cobalt alloys, as an example) [2]. In fact, its chemical combination with the host metal results in the formation of hard boron compounds that increase the property of the surface hardness. In the case of treated steels, the high surface hardness is ascribed to the formation of compact boronized layers (FeB + Fe₂B) over their surfaces. The tailored surface features for boronized steels should meet the industrial requirements. Practically, the boronizing treatment is achieved in the range of 800–1050 °C for 0.5–10 h using different sources of boron and methods: solid (paste and powder pack) [7,8], liquid [9], gas [10], plasma [11], and plasma paste [12]. Boriding in the powder medium has the main advantages of the simplicity of the process, low investment for the equipment, and cost-effectiveness [13]. During the powder-pack boriding, the samples were embedded in the powder mixture and the overall mixture was placed in the sealed hermetical recipient to prevent oxidation from

the air atmosphere. By selecting adequate process parameters, the boriding treatment was carried out in the furnace [2].

For steel, two kinds of iron borides (FeB and Fe₂B) can be formed over the surface in most cases. The Fe₂B layer is better adapted than the dual-phase borides (FeB + Fe₂B) for resisting mechanical fatigue [14]. The 4Cr5MoSiV1 steel has the same chemical composition as the versatile American AISI H13 steel. It is extensively used in hot work-tool applications. It has the capacity to withstand thermal-fatigue cracking. This steel grade also provides a high dimensional stability with excellent toughness. For example, it is employed in hot forging and extrusion dies. However, in order to prolong its lifetime during extreme working conditions, the boronizing treatment is highly recommended to improve its anti-wear property. Within the published research works, several kinetics approaches for Fe₂B layers [7,8,15–21] or dual-phase boride (FeB + Fe₂B) layers [22–30] were suggested to provide a simple tool allowing for the optimization of the layers' thicknesses to match the industrial applications. For example, in the case of Armco iron-paste boriding, Campos et al. [7] formulated the mass balance equation for the growth of an Fe₂B layer at the considered phase interface without the presence of incubation period. In another research work, Campos et al. [17] used two models (the neural network and the least square) for the kinetics of Fe₂B layers at the surface of AISI 1045 steel with a change in the boron-paste thickness. The prediction results provided a mean relative error of 5.31% for the first model and of 3.42% for the second one. Ortiz-Dominguez et al. [22] implemented two kinetics approaches (i.e., the bilayer model and the integral diffusion model) for simulating the growth of FeB and Fe₂B on AISI M2 steel in the interval of 1123 to 1273 K. Both models were checked out experimentally for validation by using two other sets of processing parameters (1243 and 1273 K for 10 h). The predicted layers' thicknesses were in accordance with the experimental values. Torres et al. [23] employed dimensional analysis for the paste boriding kinetics of AISI M2 and AISI 1045 steels by modifying the boron-paste thickness of 3 to 5 mm. Under these circumstances, three different dimensionless groups were formed for each boride layer and a power-law fitting of experimental data was used to predict the thicknesses of the FeB and Fe₂B layers. The relative error was about 16% for the FeB-layer thickness, whereas for the Fe₂B layer, the corresponding value was close to 10% for AISI M2 and AISI 1045 steels. In the present work, the same approach, already used for the paste boriding treatment by Torres et al. [23], was applied by introducing two distinct dimensionless groups needed for predicting the layers' thickness on 4Cr5MoSiV1 steel. This approach was implemented for the first time in the case of powder-pack boriding, in which the thickness of each layer depended on the boron concentration, the time duration, the parabolic growth constant, and the maximum boron penetration within the matrix for a fixed processing temperature. Keddam and Kulka [28] presented two different approaches (the average diffusion coefficient model and the Dybkov model) to study the kinetics of FeB and Fe₂B layers on AISI D2 steel in the range of 1223–1273 K. In addition, the two models' results were compared to the experimental layers' thicknesses obtained at 1243 K for 2, 4, and 6 h. A good concordance was noticed between the experiments and the predicted results. In another research paper, Mebarek and Keddam [29] used the two artificial intelligence techniques (i.e., fuzzy logic and neural network) for the simulation of layer thickness on Fe-Cr at 15 at.% Cr. The simulation results provided average relative errors of 3% for FeB and 3.5% for Fe₂B.

This work is aimed at modelling the growth kinetics of the two iron boride layers (FeB and Fe₂B) obtained from the powder-pack (solid) boronizing of 4Cr5MoSiV 1 steel. Two distinct approaches were adapted for this purpose. The model based on the dimensional analysis, which was applied for the first time for the powder-pack boriding, allowed for the prediction of the layers' thicknesses. The second approach called upon the bilayer model. This model, in its simple formulation, required the use of two new dimensionless parameters that determine the parabolic nature of the layers' growth. It was employed to estimate the boron activation energies in both iron borides (FeB and Fe₂B) for

the 4Cr5MoSiV1 steel. The obtained values of activation energies were interpreted on the basis of the literature results.

2. Diffusion Models

2.1. Bilayer Diffusion Model

The bilayer model [22,30] has been proposed for modelling the kinetics of the bilayer (FeB/Fe₂B) over the surface of 4Cr5MoSiV1 steel. This model relies on the solutions of mass balance equations at the two growing FeB/Fe₂B and Fe₂B/substrate interfaces. It assumes the linearity of boron concentration within each boride phase. The effect of incubation times was overlooked. Figure 1 shows a schematic representation of developing boron concentration profiles during the generation of iron boride layers. This figure illustrates the change in the incremental thickness for each layer within a small time step. In fact, the absorption rate of boron atoms at the surface/steel interface was rapid compared to the diffusion rate of boron atoms through the steel surface. After a certain period of time, borides' crystals appeared and came into contact to cover the steel surface by giving rise to the compact boronized layer. However, the boride incubation time was not considered in the calculations.

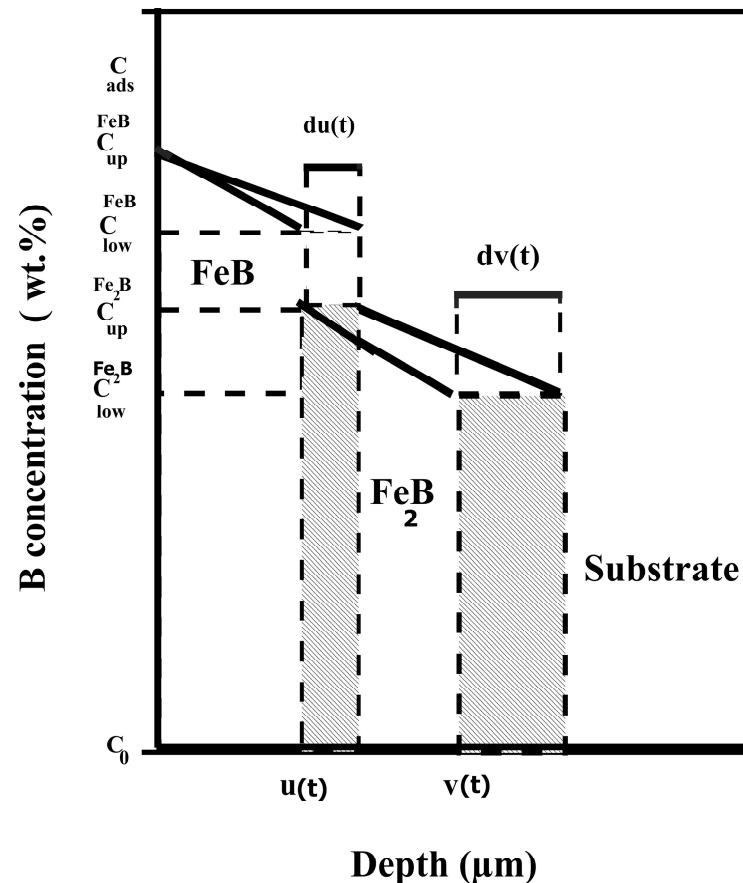


Figure 1. A schematic distribution of boron concentration profiles for the bilayer FeB/Fe₂B over the 4Cr5MoSiV1 steel.

The boron concentrations with low and upper limits were the following: C_{up}^{FeB} (=16.40 wt.% B), C_{low}^{FeB} (=16.23 wt.% B) for the FeB phase, and $C_{up}^{Fe_2B}$ (=9 wt.% B) and $C_{low}^{Fe_2B}$ (=8.83 wt.% B) for the Fe₂B phase [22,23]. The variable $u(t)$ is the position of the first interface, and $v(t)$ refers to that of the second interface. C_{ads} is the required boron content being adsorbed at the onset of a process [25]. C_0 represents the solubility limit of boron in the matrix, which

is equal to 35×10^{-4} wt.% B [31]. The change in time of the FeB layer's thickness follows Equation (1).

$$u(t) = k' \sqrt{t} = 2\zeta \sqrt{D_{FeB} t} \quad (1)$$

where k' is the kinetic constant of the first interface with a dimensionless parameter of value ζ . D_{FeB} stands for the value of the boron diffusion coefficient in FeB for a given processing temperature. The thickness of the entire boronized layer (FeB + Fe₂B) represented by the distance $v(t)$ is expressed by Equation (2).

$$v(t) = k \sqrt{t} = 2\eta \sqrt{D_{Fe_2B} t} \quad (2)$$

where k designates the kinetic constant of the second interface with a dimensionless parameter of value η . The parameter D_{Fe_2B} represents the value of the boron diffusion coefficient in Fe₂B for the given boronizing temperature. The bilayer model [22,30] is governed by the set of ordinary differential equations of the first order provided by Equations (3) and (4):

$$w_1 \frac{du(t)}{dt} = D_{FeB} \left(\frac{C_{up}^{FeB} - C_{low}^{FeB}}{u(t)} \right) - D_{Fe_2B} \left(\frac{C_{up}^{Fe_2B} - C_{low}^{Fe_2B}}{(v(t) - u(t))} \right) \quad (3)$$

$$w_2 \frac{dv(t)}{dt} + w_{12} \frac{du(t)}{dt} = D_{Fe_2B} \left(\frac{C_{up}^{Fe_2B} - C_{low}^{Fe_2B}}{(v(t) - u(t))} \right) \quad (4)$$

where

$$w_1 = \left[\frac{(C_{up}^{FeB} + C_{low}^{FeB})}{2} - C_{up}^{Fe_2B} \right] \quad w_2 = \left[\frac{(C_{up}^{Fe_2B} + C_{low}^{Fe_2B})}{2} - C_0 \right]$$

and

$$w_{12} = \frac{(C_{up}^{Fe_2B} - C_{low}^{Fe_2B})}{2}$$

During the mathematical formulation of the bilayer model, certain assumptions were considered as follows: (a) The diffusion phenomenon occurs in the domain of one dimension, (b) the boron concentrations remain constant and are independent of time at the phase fronts, (c) the boron diffusivity in each phase byes the Arrhenius equation, and (d) the layer thickness is smaller than the diffusion depth. The mass flux of boron atoms through the steel matrix is negligible due to the small solubility of boron in the iron phase. By derivation of Equations (1) and (2) with respect to the time duration and after substituting them into the two ordinary differential equations (i.e., Equations (3) and (4)), the expressions of the two dimensionless parameters ζ and η could easily be derived as follows:

$$\zeta = \sqrt{\frac{k'(C_{up}^{FeB} - C_{low}^{FeB})}{2[(w_1 + w_{12})k' + w_2k]}} \quad (5)$$

$$\eta = k \sqrt{\frac{w_{12}}{(w_2k + w_{12}k')(k - k')}} \quad (6)$$

This makes possible to deduce the expressions of the boron diffusion coefficients in FeB and Fe₂B as follows:

$$D_{FeB} = \left(\frac{k'}{2\zeta} \right)^2 \quad (7)$$

and

$$D_{Fe_2B} = \left(\frac{k}{2\eta} \right)^2 \quad (8)$$

Equations (7) and (8) were deduced from Equations (1) and (2), respectively.

2.2. The Approach Based on the Dimensional Analysis

The kinetic approach based on the dimensional analysis can be applied to analyze the time dependencies of the thicknesses of FeB and Fe₂B layers on this type of steel. After the Pi-Buckingham theorem [32], any physical problem depending on N variables with p fundamental units can be described by forming $(N - p)$ dimensionless groups Π_{N-p} , so each dimensional group can be written as a function of others. For instance, the i -th dimensional group Π_i can be written as follows: $\Pi_i = \Pi_i(\Pi_1, \Pi_2, \dots, \Pi_{i-1}, \Pi_{i+1}, \dots, \Pi_{N-p})$, for $i = 1, N - p$, and the same applies to other dimensional groups. For the sake of simplicity, the given dimensionless group Π_i can be expressed as a function of other dimensionless groups by using the products of power laws. These relationships, based on the power laws and including all the involved dimensionless groups, have already been used to describe the kinetics of boronizing process [19,23]. In addition, the fitting of experimental data according to the power law is a general trend for approaching the observed classical parabolic law with an exponent being close to 0.5. Such behavior in terms of kinetics is experienced in many studies regarding the boriding of steels [7–30]. Each boride layer thickness u or l , where $l = (v - u)$, depends on the following variables: the parabolic growth constant of FeB, where $k_1 = k'$, or that of Fe₂B, for which $k_2 = (k - k')$; the maximum depth of boron penetration λ_{\max} ; the boron concentration in the FeB or Fe₂B layer; C_{FeB} or C_{Fe_2B} ; and the time duration t for the given process temperature $u = u(k_1, t, C_{FeB}, \lambda_{\max})$ and $l = l(k_2, t, C_{Fe_2B}, \lambda_{\max})$. For indication, the diffusion distance λ_{\max} stands for the maximum depth of boron atom diffusion across the material surface in the absence of an iron boride layer. It can be determined by using the following relation: $\lambda_{\max} = \sqrt{D(T_{\max})t_{\max}}$, where $D(T_{\max})$ is the value of the boron diffusion coefficient in the iron phase [26] at $T = T_{\max}$ for a maximum time duration of the boriding process. It is noted that the maximum processing temperature within the selected range occurs in the austenite phase. The boron diffusion coefficient in the γ -Fe phase [26] is given by Equation (9) and is valid for $T > 1184.6$ K:

$$D = 4.4 \times 10^{-8} \exp\left(-\frac{81.5kJ}{RT}\right) \quad (9)$$

where T is the temperature expressed in Kelvin, and $R = 8.314 \text{ J mol}^{-1}\text{K}^{-1}$ represents the ideal gas constant. In the dimensional analysis, the studied system involved five variables with three fundamental units, which provide two dimensionless groups for each layer thickness u or l . Applying the principle of dimensional analysis for FeB layer thickness, the two dimensionless groups $\Pi_{11} = \frac{u}{\lambda_{\max}}$ and $\Pi_{12} = t\left(\frac{k'}{\lambda_{\max}}\right)^2$ are obtained. In the same way, the two dimensionless groups $\Pi_{21} = \frac{l}{\lambda_{\max}}$ and $\Pi_{22} = t\left(\frac{k-k'}{\lambda_{\max}}\right)^2$ can also be deduced from the measurement of Fe₂B layer thickness. For predicting the thickness of each layer, a fitting of experimental data according to the power law [19,23] can be used as follows:

$$\Pi_{11} = \alpha_1 \Pi_{12}^{\beta_1} \quad (10)$$

$$\Pi_{21} = \alpha_2 \Pi_{22}^{\beta_2} \quad (11)$$

where the coefficients α_1 , α_2 , β_1 , and β_2 are determined from the fitting of the experimental results using Relations (10) and (11). These coefficients do not change significantly with the process temperature. Therefore, their mean arithmetic values can be taken for the simulation of boronizing kinetics on the basis of dimensional analysis. In addition, the experimental parabolic growth constants k' and k can be fitted by employing the two Arrhenius relationships as follows: $k' = \exp\left(\frac{a_1}{T} + b_1\right)$ and $k = \exp\left(\frac{a_2}{T} + b_2\right)$, where the constants a_1 , a_2 , b_1 , and b_2 are the fitting parameters. Finally, the expressions of the predicted layers' thicknesses u and v for FeB and FeB + Fe₂B are given by Equations (12) and (13), respectively:

$$u = \frac{\alpha_1 t^{\beta_1}}{\lambda_{\max}^{(2\beta_1-1)}} \left(\exp\left(\frac{a_1}{T} + b_1\right)\right)^{2\beta_1} \quad (12)$$

$$v = \frac{\alpha_2 t^{\beta_2}}{\lambda_{\max}^{(2\beta_2-1)}} \left(\exp\left(\frac{a_2}{T} + b_2\right) - \exp\left(\frac{a_1}{T} + b_1\right) \right)^{2\beta_2} + u \quad (13)$$

In addition, the respective values of boron activation energies Q_1 and Q_2 in FeB and Fe₂B can be deduced experimentally from the squared values of k' and k with $Q_1 = -2a_1R$ and $Q_2 = -2a_2R$, respectively, where R denotes the ideal gas constant with $R = 8.314 \text{ J mol}^{-1}\text{K}^{-1}$.

3. Calculation Results and Discussions

The experimental results obtained by Delai et al. [27] were exploited to analyze kinetically the powder-pack boronizing process of 4Cr5MoSiV1 steel, whose chemical composition was not provided in their paper. The steel-grade steel, which is a Chinese brand of American AISI H13 steel, has the nominal chemical composition of 0.32–0.45 wt.% C, 4.75–5.50 wt.% Cr, 1.10–1.75 wt.% Mo, 0.8–1.20 wt.% Si, 0.80–1.20 wt.% V, 0.20–0.50 wt.% Mn, 0.30 wt.% Ni, 0.25 wt.% Cu, 0.30 wt.% P, and 0.30 wt.% S and Fe balance. For useful experimental details, the powder-pack boronizing treatment was carried out in the interval of 1133 to 1253 K for variable time durations (1, 2, 4, 6, and 8 h). The reactive medium was in the solid state and composed of 5 wt.% B₄C, 4 wt.% KBF₄, 5 wt.% C, and 88 wt.% SiC. The specimens to be treated were put into a hermetical recipient made of stainless steel and embedded in the powder mixture. The processing temperatures were set as 1133, 1173, 1213, and 1253 K for 1–8 h. When the process was finished, the recipient was taken out of the muffle furnace and air cooled. The analysis of kinetic data [27] overlooked the occurrence of boride incubation times. These experimental data [27] allowed us to generate plots relating the layers' thicknesses as a function of the square root of the time. Table 1 shows the deduced values of the kinetics constants relative to the two growth fronts in the temperature range of 1133–1253 K. The experimentally deduced values of k' and k from the kinetics curves changed with the processing temperature, indicating the acceleration of the diffusion rates of boron atoms at elevated temperatures because the phenomenon of boron diffusion is a thermally activated process.

Table 1. Derivation of parabolic growth constants from the experimental results [27] in the range of 1133 to 1253 K.

T (K)	k' ($\mu\text{m s}^{-0.5}$)	k ($\mu\text{m s}^{-0.5}$)
1133	0.0905	0.2377
1173	0.1318	0.3180
1213	0.1680	0.4237
1253	0.2169	0.5247

3.1. Evaluation of Diffusion Coefficients of Boron in FeB and Fe₂B Using the Bilayer Model

The player model involving two unitless parameters ζ and η can be exploited to determine the boron diffusion coefficient in each phase. First, the numerical values of these two dimensionless parameters were calculated from Equations (5) and (6), respectively. Afterward, the calculated boron diffusion coefficients in FeB and Fe₂B displayed in Table 2 were obtained from Equations (7) and (8), respectively using experimental data [27] in terms of kinetics constants at the growing interfaces.

Table 2. Calculated boron diffusion in FeB and Fe₂B together with unitless parameters with the bilayer model.

T (K)	$D_{\text{FeB}} \times 10^{-12}$ (m^2s^{-1})	$D_{\text{Fe}_2\text{B}} \times 10^{-12}$ (m^2s^{-1})	ζ Parameter	η Parameter
1133	0.74	0.92	0.0525	0.1238
1173	1.48	1.56	0.0542	0.1273
1213	2.48	2.85	0.0533	0.1254
1253	4.00	4.25	0.0541	0.1272

To obtain the value of boron activation energy in each boride phase, the calculated boron diffusion coefficients in iron borides from Table 2 were fitted with Arrhenius relations. The two unitless parameters were nearly constant ($\xi \approx 0.053$ and $\eta \approx 0.1259$) for the considered boriding temperatures. This result confirmed the parabolic trend during the growth of two layers, FeB and Fe₂B. Such a behavior corroborated the parabolic nature of the layers' growth. The temperature dependencies of diffusion coefficients of boron in FeB and Fe₂B shown in Figure 2 are given by Equations (14) and (15), respectively:

$$D_{FeB} = 3.09 \times 10^{-5} \exp\left(\frac{-164.92 \text{ kJ mol}^{-1}}{RT}\right) \quad (14)$$

$$D_{Fe_2B} = 1.08 \times 10^{-5} \exp\left(\frac{-153.39 \text{ kJ mol}^{-1}}{RT}\right) \quad (15)$$

with $R = 8.314 \text{ J mol}^{-1} \text{ K}^{-1}$ and T is the process temperature in Kelvin. For applying the based dimensional analysis model, the time dependencies of parabolic growth constants were therefore necessary for the calculation. The corresponding expressions of k' and k are provided by Equations (16) and (17), respectively, after the experimental values of Table 1 were fitted with Arrhenius relations:

$$k' = \exp\left(-\frac{10190.16}{T} + 6.6184\right) \quad (16)$$

$$k = \exp\left(\frac{-9461.11}{T} + 6.9201\right) \quad (17)$$

The temperature-dependent parameters k' and k are expressed in $\mu\text{m s}^{-0.5}$ and T represents the boriding temperature in Kelvin. The Q_1 and Q_2 parameters are the boron activation energies in FeB and Fe₂B to be deduced from the squares of Equations (16) and (17), respectively, based on the experimental results [27]. The calculated values of activation energies in FeB and Fe₂B were equal to 169.44 and 157.32 kJ mol⁻¹, respectively.

Table 3 groups the different values of boron activation energies obtained on some alloyed borided steels [22,27,33–42] and compares them to the present results from the bilayer model. It is seen from Table 3 that the values of the activation energies were affected by several factors. These factors may include the following: the boriding method employed, the chemical composition of steels, the temperature range utilized, the heating source, the composition of the reacting medium and its physical state, the method of calculation, and even the presence of grooves with different shapes on the treated steels. As an illustrative example, Rafidah et al. [43] machined different geometrical shapes of grooves on the cubic samples of treated mild steel. These samples were pack boronized at 1123, 1173, and 1223 K for 2, 4, and 6 h. In case of powder-pack boronized high-alloy steels [22,38,39,41], the obtained activation energies were high compared to the plasma-paste boriding [33,34]. For the powder-pack boriding, a plausible explanation could be the change in the values of the boron activity in the contact area between the powder mixture and the steel surface during the process, which could have drastically lowered the diffusion rate of boron atoms inside the substrate. As a consequence, the values of the energetic barriers (in terms of activation energies) of the system would have increased.

In fact, the presence of alloying elements with high contents had a great impact on the growth rate of boron atoms in the solid boronizing process [22,38,39,41,42], which reduced the layer's thicknesses with the presence of metal borides. On the other hand, the use of the plasma-paste process allows for a reduction in activation energies because of the activation of the generated plasma [33,34] even in the case of AISI 304 and AISI 440C steels.

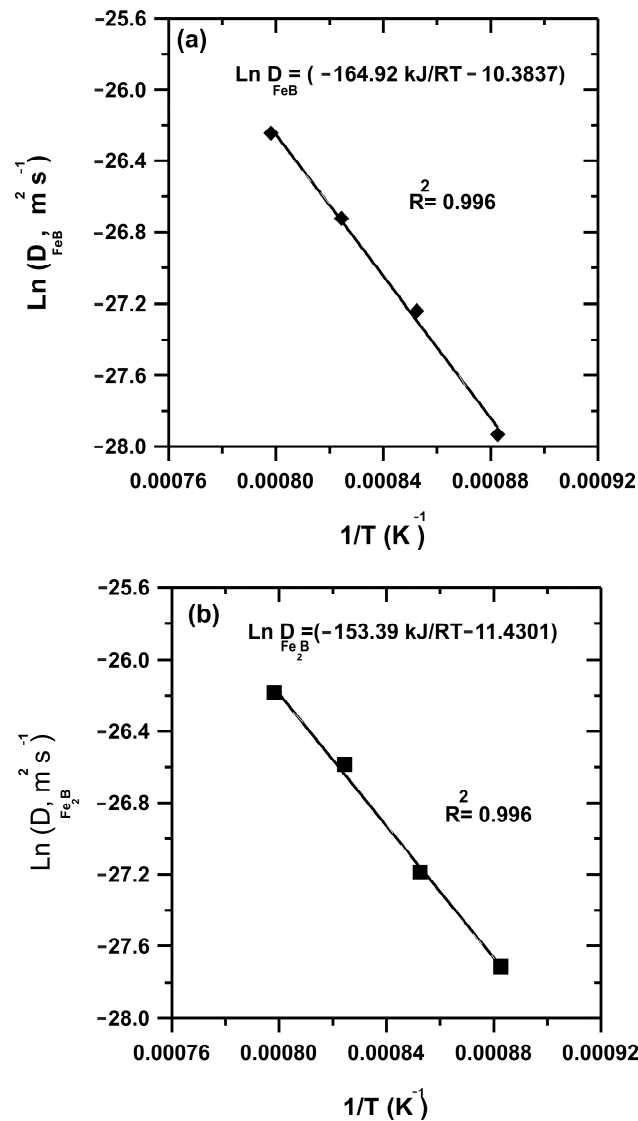


Figure 2. Temperature dependency of calculated boron diffusion coefficient in each layer with the bilayer model: (a) FeB layer and (b) Fe_2B layer.

Even though the plasma-paste boriding enabled adequate thicknesses of the boronized layers at low temperature (i.e., 700 °C) to be obtained in the laboratories as a result of overactivation of the plasma, its application in the industry has not been implemented till now. In fact, plasma-paste boriding is not currently employed at an industrial scale due to the high cost of investment and cannot be applied for treating large workpieces. Therefore, the use of this boriding technique is exclusively limited to the laboratory scale.

They reported that the groove shape had a manifest influence on the values of boron activation energies ranging from 76.51 and 244.36 kJ mol^{-1} . They explained the obtained results were due to the difference in the growth rate of boron atoms during the contact with the groove surface. Campos-Silva et al. [37] designed a new process called pulsed direct current powder-pack boriding, in which the diffusion phenomenon of boron atoms was enhanced under the effect of an electrical field and resulted in the reduction of activation energies in FeB and Fe_2B for the AISI 316 L steel compared to conventional powder-pack boriding [22,38,39,41]. Delai et al. [27] used different powder mixtures comparatively to other compositions of powders [22,38,39,41] to treat the 4Cr5MoSiV1 steel and obtained the following activation energies: 205.25 and 170.915 kJ mol^{-1} in FeB and Fe_2B , respectively. When scrutinizing their computation results from the employed model, an inconsistency was noticed. In fact, the boron activation energies in FeB and Fe_2B reported by

Delai et al. [27] were at all not correct. A careful verification of their calculations led to different values, which were, respectively, 149.55 and 148.84 kJ mol⁻¹ after taking the value of 27.26 wt. % as an upper limit of boron in FeB. Such a value of concentration is even inconsistent with the experimental binary-phase diagram Fe-B regarding the composition range of the FeB phase, which is very narrow and located between 16.23 and 16.40 wt.%. It is worth mentioning that the value of 27.26 wt.% B in FeB had a direct effect on the calculation results of the activation energies. Despite this fact, the revised values of the boron activation energies in both phases from our calculations are in accordance with the present results, with a comparable magnitude order. Unexpectedly, Delai et al. [27] compared the experimental thicknesses with the predicted values by using their model. They showed a good agreement with the experiments in spite of the incorrectness of the calculated values of the activation energies. In fact, they performed a simple adjustment of the two dimensionless parameters (ζ and η) of their model, which were also incorrect, to claim the validity of their approach. Based on our model and the classical parabolic growth law, the assessed boron activation energies in both phases listed in Table 3 are very comparable. The calculation was completed with values of the dimensionless parameters (ζ and η) that were completely different from those of Ref. [27], which were incorrect (see Table 2), with an upper boron concentration in FeB of 16.40 wt.%. Consequently, our obtained results in terms of activation energies are now compatible with each other.

Table 3. Comparison of the determined values of boron activation energies on some alloyed borided steels with the literature data.

Steel	Boriding Process	Temperature Range (K)	Activation Energy (Kj mol ⁻¹)	Method of Calculation	Refs.
AISI 304	Plasma	1023–1223	123	Parabolic growth law	[33]
AISI 440C	Plasma paste	973–1073	134.62	Parabolic growth law	[34]
AISI T1	CRTD-Bor	1123–1323	179	Parabolic growth law	[35]
AISI D2	Salt bath	1223–1273	170	Parabolic growth law	[36]
AISI 316L	Pulsed DC	1123–1223	162 (FeB), 171 (FeB)	Bilayer model	[37]
AISI M2	Paste with different paste thickness	1193–1273	255.76 (FeB), 201.0 (FeB)	Bilayer model	[42]
AISI 316L	Powder with microwave heating	1073–1223	244.15	Parabolic growth law	[38]
AISI H13	Powder with two mixtures	1073–1223	227.5 with nano-boron 284.2 with Ekabor II	Parabolic growth law	[39]
AISI H13	Powder	1123–1223	185.7	Parabolic growth law	[40]
AISI H13	Powder	1173–1273	236.43 (FeB) 233.04 (Fe ₂ B)	Mean Diffusion coefficient method	[41]
AISI M2	Powder	1123–1273	220.5 (FeB) 210.90 (Fe ₂ B)	Bilayer model	[22]
4Cr5MoSiV1	Powder	1133–1253	205.25 (FeB) 170.915 (Fe ₂ B)	Bilayer model	[27]
4Cr5MoSiV1	Powder	1133–1253	164.92 (FeB) 153.39 (Fe ₂ B)	Bilayer model	This work
4Cr5MoSiV1	Powder	1133–1253	169.44 (FeB) 157.32 (Fe ₂ B)	Parabolic growth law	This work

3.2. Prediction of Layers' Thicknesses with the Base Dimensional Analysis Model

To validate the base dimensional analysis model, the two dimensionless groups attributed to each boride layer needed to be related to each other by using an experimental fitting of the experimental data with a nonlinear regression described by the power laws given by Equations (10) and (11). First, the value of maximum boron penetration in the steel substrate needed to be determined. This corresponds to the maximum diffusion distance into the steel substrate in the absence of iron boride formation. A simple calculation of λ_{\max} at 1253 K for the prolonged time duration of 8 h yielded a value of 712 μm based on the diffusivity of boron in the γ -Fe phase given in Ref. [26]. Figure 3 shows the evolution of the dimensionless group Π_{11} or Π_{21} versus Π_{12} or Π_{22} for each boride layer. The results of this nonlinear fitting are summarized in Table 4. The obtained fitting curves plotted in Figure 3 confirmed the parabolic regime regarding the growth kinetics of FeB and Fe₂B

since the arithmetic mean values of β_1 and β_2 were, respectively, 0.5259 and 0.5469, which are typically close to the characteristic value of 0.5 observed in the classical parabolic growth law. In addition, the arithmetic mean values of α_1 and α_2 deduced from Table 4 were, respectively, equal to 1.2605 and 1.4368.

Figure 4 shows the plots of the time dependencies of the layers' thicknesses by comparing the experimental results with those obtained from the dimensional analysis employing Equations (12) and (13) as well as the predicted values of the bilayer model. It can be seen that the predicted values of the layers' thicknesses by both approaches are concordant with the experiments. However, the prediction results from the bilayer model were closer to the experimental data [27] compared to those derived from the dimensional analysis. In this model, which used dimensional analysis, the reason for some slight observed discrepancies between the experiments and the calculations concerning the total boride ($\text{FeB} + \text{Fe}_2\text{B}$)-layer thickness for a treatment duration exceeding 4 h could be ascribed to the use of mean values of fitting coefficients α_1 , α_2 , β_1 , and β_2 . Despite this fact, the approach based on the dimensional analysis is still suitable for modelling the growth kinetics of boride layers generated at the surfaces of the 4Cr5MoSiV1 steel.

The advantage of using dimensional analysis lies in its simple mathematical formulation. It can be extended to a multiphase system and applied to any thermochemical process. The bilayer model also shows the possibility of kinetically describing the evolution of layers' thicknesses for a given processing temperature. However, it did not account for the presence of metal borides as precipitates, which could hamper the diffusion of an interstitial element (boron) over greater depth. The mutual chemical interaction (carbon–boron) was also overlooked because the boron atoms competed with carbon atoms to occupy the octahedral sites in the lattices of iron borides. As a consequence, the carbon element was pushed away from the boronized layer and was concentrated in the transition zone, as in case of the 4Cr5MoSiV1 steel.

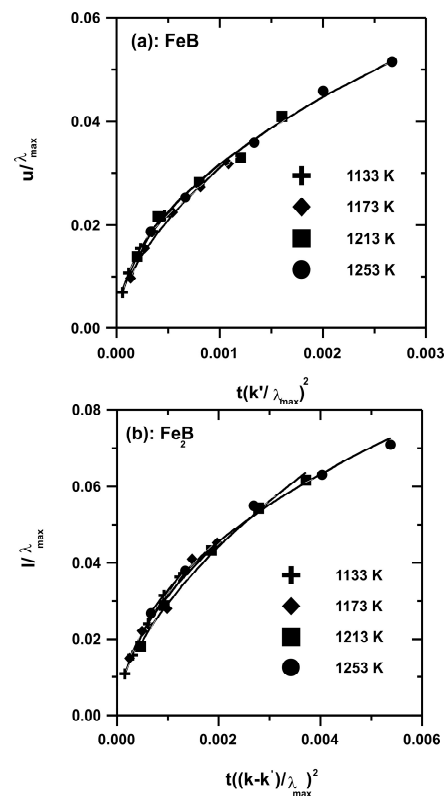


Figure 3. Relationships between the dimensionless groups in each layer: (a) FeB and (b) Fe_2B .

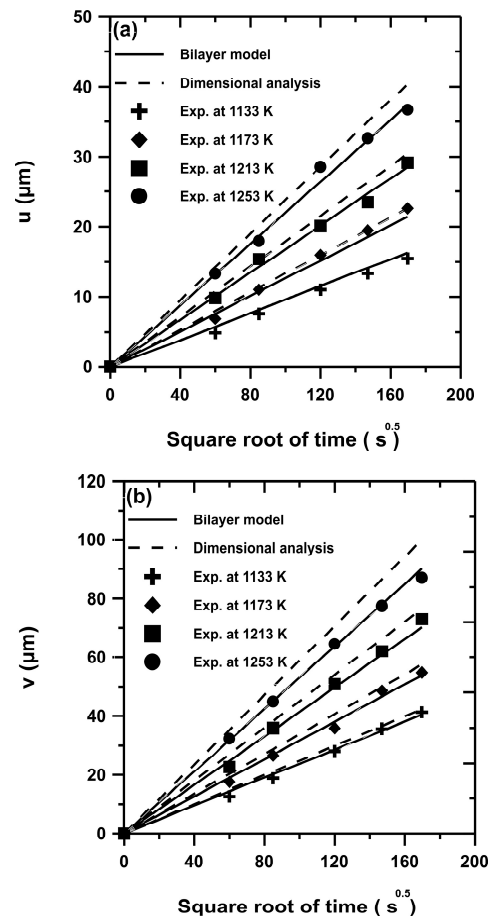


Figure 4. Relationships between the dimensionless groups in each layer: (a) FeB and (b) Fe₂B.

Table 4. Identification of the constants involved in Equations (10) and (11) by using a non-linear fitting of the experimental data [27].

T (K)	α_1 for FeB	β_1 for FeB	α_2 for FeB	β_2 for FeB
1173	1.4855	0.5483	1.9113	0.5910
1223	1.6194	0.5649	1.2415	0.5329
1273	0.9540	0.4929	1.7308	0.5903
1323	0.9831	0.4975	0.8637	0.4736

4. Conclusions

In this work, a simulation was carried out on the boronizing kinetics of 4Cr5MoSiV1 steel in the interval of 1133 to 1253 K. Two kinetics approaches were employed to attain this objective. The concluding points can be drawn as follows from this simulation work:

- (1) The bilayer model based on the principle of mass conservation at each phase front was used to assess the diffusion coefficients of boron in FeB and Fe₂B.
- (2) The calculation from the bilayer model shows that the values of the two dimensionless parameters ($\zeta \approx 0.053$ and $\eta \approx 0.1259$) were nearly constant within the considered temperature range. This outcome confirms the parabolic character during the layers' growth.
- (3) The calculation results from the bilayer model were fitted with Arrhenius relations to derive the values of activation energies in both phases (FeB and Fe₂B), which were, respectively, 164.92 and 153.39 kJ mol⁻¹.

- (4) The obtained activation energies with the bilayer model were very comparable to the values derived from the classical parabolic growth law, which were $169.44 \text{ kJ mol}^{-1}$ for FeB and $157.32 \text{ kJ mol}^{-1}$ for Fe₂B.
- (5) The based dimensional analysis model and the bilayer model were capable of predicting the layers' thicknesses, whose values were concordant with the experimental results taken from the literature.
- (6) Two dimensionless groups were derived during the establishment of the kinetic model based on the dimensional analysis. The experimental results were fitted according to the power laws to express the interdependence of the two dimensionless parameters.
- (7) The kinetic approach based on dimensional analysis showed its versatility and capability of analyzing the boronizing kinetics of 4Cr5MoSiV1 steel.
- (8) In future works, both kinetics approaches could be potentially used to model the diffusion phenomenon of interstitial elements such as boron or nitrogen in a multi-phase system (ferrous or non-ferrous alloys).

Author Contributions: Conceptualization, K.B. and M.K. (Mourad Keddám); data curation, K.B., M.K. (Mourad Keddám) and B.B.; formal analysis, K.B. and M.K. (Mourad Keddám); funding acquisition, M.K. (Mourad Keddám); investigation, K.B., M.K. (Mourad Keddám) and B.B.; methodology, K.B., M.K. (Mourad Keddám), B.B. and M.K. (Michał Kulka); project administration, M.K. (Mourad Keddám); resources, K.B. and M.K. (Mourad Keddám); supervision, K.B. and M.K. (Mourad Keddám); validation, K.B. and M.K. (Mourad Keddám); visualization, K.B., M.K. (Mourad Keddám), B.B. and M.K. (Michał Kulka); writing—original draft, K.B. and M.K. (Mourad Keddám); writing—review and editing, K.B., M.K. (Mourad Keddám) and M.K. (Michał Kulka). All authors have read and agreed to the published version of the manuscript.

Funding: This research received no external funding. This work was carried out within the PRFU project registered under number A11N01UN160420230012. It was supported by the Ministry of Higher Education and Scientific Research of Algeria and coordinated by the DGRSDT, Algeria. In the part realized by Michał Kulka this research was funded by the Ministry of Science and Higher Education in Poland, grant number 0513/SBAD/4797.

Institutional Review Board Statement: Not applicable.

Informed Consent Statement: Not applicable.

Data Availability Statement: Not applicable.

Conflicts of Interest: The authors declare no conflict of interest.

References

1. Campos-Silva, I.E.; Rodríguez-Castro, G.A. *Boriding to Improve the Mechanical Properties and Corrosion Resistance of Steels, Thermochemical Surface Engineering of Steels*, 1st ed.; Mittemeijer, E.J., Somers, M.A.J., Eds.; Woodhead-Elsevier Publishing: Cambridge, UK, 2015; pp. 651–697.
2. Kulka, M. *Current Trends in Boriding: Techniques*; Springer International Publishing: Cham, Switzerland, 2019.
3. Pashechko, M.; Dziedzic, K.; Jozwik, J. Analysis of Wear Resistance of Borided Steel C45. *Materials* **2020**, *23*, 5529. [[CrossRef](#)]
4. Allaoui, L.A.; Allaoui, O. Corrosion resistance of borided layers obtained on XC38 steel. *Indian J. Eng. Mater. Sci.* **2018**, *25*, 421–424.
5. Kartal, G.; Kahvecioglu, O.; Timur, S. Investigating the morphology and corrosion behavior of electrochemically borided steel. *Surf. Coat. Technol.* **2006**, *200*, 3590–3593. [[CrossRef](#)]
6. Salyi, Z.; Kaptay, G.; Koncz-Horvath, D.; Somlyai-Sipos, L.; Zoltan Kovacs, P.; Lukacs, A.; Marton, B. Boride Coatings on Steel Protecting it Against Corrosion by a Liquid Lead-Free Solder Alloy. *Metall. Mater. Trans. B* **2022**, *53*, 730–743. [[CrossRef](#)]
7. Campos, I.; Oseguera, J.; Figueroa, U.; García, J.A.; Bautista, O.; Kelemenis, G. Kinetic study of boron diffusion in the paste-boriding process. *Mater. Sci. Eng. A* **2003**, *352*, 261–265. [[CrossRef](#)]
8. Ortiz-Domínguez, M.; Gómez-Vargas, O.A.; Bárcenas-Castañeda, M.; Castellanos-Escamilla, V.A. Comparison and Analysis of Diffusion Models: Growth Kinetics of Diiron Boride Layers on ASTM A283 Steel. *Materials* **2022**, *23*, 8420. [[CrossRef](#)] [[PubMed](#)]
9. Smol'nikov, E.A.; Sarmanova, L.M. Study of the possibility of liquid boriding of high-speed steels. *Met. Sci. Heat Treat.* **1982**, *24*, 785–788. [[CrossRef](#)]
10. Kulka, M.; Makuch, N.; Piasecki, A. Nanomechanical characterization and fracture toughness of FeB and Fe₂B iron borides produced by gas boriding of Armco iron. *Surf. Coat. Technol.* **2017**, *325*, 515–532. [[CrossRef](#)]

11. Sikorski, K.; Wierzchoń, T.; Bielinski, P. X-ray microanalysis and properties of multicomponent plasma-borided layers on steels. *J. Mater. Sci.* **1998**, *33*, 811–815. [[CrossRef](#)]
12. Gunes, I.; Ulker, S.; Taktak, S. Plasma paste boronizing of AISI 8620, 52100 and 440C steels. *Mater. Des.* **2011**, *32*, 2380–2386. [[CrossRef](#)]
13. Jain, V.; Sundararajan, G. Influence of the pack thickness of the boronizing mixture on the boriding of steel. *Surf. Coat. Technol.* **2002**, *149*, 21–26. [[CrossRef](#)]
14. Barkat, A.; Hammou, A.D.; Allaoui, O. Effect of Boriding on the Fatigue Resistance of C20 Carbon Steel. *Acta Phys. Pol. A* **2017**, *132*, 813–815. [[CrossRef](#)]
15. Morgado-González, I.; Ortiz-Dominguez, M.; Keddám, M. Characterization of Fe₂B layers on ASTM A1011 steel and modeling of boron diffusion. *Mater. Testing.* **2022**, *64*, 55–66. [[CrossRef](#)]
16. Campos, I.; Islas, M.; González, E.; Ponce, P.; Ramírez, G. Use of fuzzy logic for modeling the growth of Fe₂B boride layers during boronizing. *Surf. Coat. Technol.* **2006**, *201*, 2717–2723. [[CrossRef](#)]
17. Campos, I.; Islas, M.; Ramírez, G.; VillaVelázquez, C.; Mota, C. Growth kinetics of borided layers: Artificial neural network and least square approaches. *Appl. Surf. Sci.* **2007**, *253*, 6226–6231. [[CrossRef](#)]
18. Ramdan, R.D.; Takaki, T.; Yashiro, K.; Tomita, Y. The Effects of Structure Orientation on the Growth of Fe₂B Boride by Multi-Phase-Field Simulation. *Mater. Trans.* **2010**, *51*, 62–67. [[CrossRef](#)]
19. Nait Abdellah, Z.; Keddám, M.; Chegroune, R.; Bouarour, B.; Lillia, H.; Elias, A. Simulation of the boriding kinetics of Fe₂B layers on iron substrate by two approaches. *Matériaux Tech.* **2012**, *100*, 581–588. [[CrossRef](#)]
20. Kouba, R.; Keddám, M.; Kulka, M. Modelling of the paste boriding process. *Surf. Eng.* **2015**, *31*, 563–569. [[CrossRef](#)]
21. Castillo-Vela, L.E.; Mejía-Caballero, I.; Rosales-Lopez, J.L.; Olivares-Luna, M.; Contreras-Hernández, A.; Keddám, M. The influence of a pulsed-DC field on the growth of the Fe₂B layer and the electrical behavior of the boriding media. *Vacuum* **2023**, *210*, 111846. [[CrossRef](#)]
22. Ortiz Domínguez, M.; Keddám, M.; Gómez Vargas, O.A.; Ares de Parga, G.; Zuno Silva, J. Bilayer growth kinetics and tribological characterization of boronized AISI M2 steel. *Mater. Test.* **2022**, *64*, 473–489. [[CrossRef](#)]
23. Torres, R.; Campos, I.; Ramírez, G.; Bautista, O.; Martínez, J. Dimensional analysis in the growth kinetics of FeB and Fe₂B layers during the boriding process. *Int. J. Microstruct. Mater. Prop.* **2007**, *2*, 73–83.
24. Keddám, M.; Kulka, M. Simulation of the growth kinetics of FeB and Fe₂B layers on AISI D2 steel by the integral method. *Phys. Met. Metallogr.* **2018**, *119*, 842–851. [[CrossRef](#)]
25. Yu, L.; Chen, X.; Khor, K.; Sundararajan, G. FeB/Fe₂B phase transformation during SPS pack-boriding: Boride layer growth kinetics. *Acta Mater.* **2005**, *53*, 2361–2368. [[CrossRef](#)]
26. Keddám, M.; Chentouf, S.M. A diffusion model for describing the bilayer growth (FeB/Fe₂B) during the iron powder-pack boriding. *Appl. Surf. Sci.* **2005**, *252*, 393–399. [[CrossRef](#)]
27. Delai, O.; Xia, C.; Shiqiang, L. Growth kinetics of the FeB/Fe₂B boride layer on the surface of 4Cr5MoSiV1 steel: Experiments and modelling. *J. Mater. Res. Technol.* **2021**, *11*, 1272–1280. [[CrossRef](#)]
28. Keddám, M.; Kulka, M. Simulation of Boriding Kinetics of AISI D2 Steel using Two Different Approaches. *Met. Sci. Heat Treat.* **2020**, *61*, 756–763. [[CrossRef](#)]
29. Mebarek, B.; Keddám, M. A fuzzy neural network approach for modeling the growth kinetics of FeB and Fe₂B layers during the boronizing process. *Matériaux Tech.* **2018**, *106*, 603. [[CrossRef](#)]
30. Roy, U. Phase boundary motion and polyphase diffusion in binary metal-interstitial systems. *Acta Metall.* **1968**, *16*, 243–253. [[CrossRef](#)]
31. Okamoto, H. B-Fe (boron-iron). *J. Phase Equilibria Diffus.* **2004**, *25*, 297–298. [[CrossRef](#)]
32. Bahman, Z. *Dimensional Analysis Beyond the Pi Theorem*; Springer: Cham, Switzerland, 2017; p. 266.
33. Yoon, J.H.; Jee, Y.K.; Lee, S.Y. Plasma paste boronizing treatment of the stainless steel AISI 304. *Surf. Coat. Technol.* **1999**, *112*, 71–75. [[CrossRef](#)]
34. Keddám, M.; Chegroune, R.; Kulka, M.; Panfil, D.; Ulker, S.; Taktak, S. Characterization and Diffusion Kinetics of the Plasma Paste Borided AISI 440C Steel. *Trans Indian Inst. Met.* **2017**, *70*, 1377–1385. [[CrossRef](#)]
35. Kartal Sireli, G.; Yuce, H.; Arslan, M.; Karimzadehkhoei, M.; Timur, S. Improving the Surface Performance of Discarded AISI T1 Steel by Cathodic Reduction and Thermal Diffusion-Based Boriding. *J. Mater. Eng. Perform.* **2023**, *in press*. [[CrossRef](#)]
36. Sen, S.; Sen, U.; Bindal, C. An approach to kinetic study of borided steels. *Surf. Coat. Technol.* **2005**, *191*, 274–285. [[CrossRef](#)]
37. Campos-Silva, I.; Hernández-Ramírez, E.J.; Contreras-Hernández, A.; Rosales-Lopez, J.L.; Valdez-Zayas, E.; Mejía-Caballero, I.; Martínez-Trinidad, J. Pulsed-DC powder-pack boriding: Growth kinetics of boride layers on an AISI 316 L stainless steel and Inconel 718 superalloy. *Surf. Coat. Technol.* **2021**, *421*, 127404. [[CrossRef](#)]
38. Ipek Ayvaz, S.; Aydin, I. Effect of the Microwave Heating on Diffusion Kinetics and Mechanical Properties of Borides in AISI 316L. *Trans. Indian Inst. Met.* **2020**, *73*, 2635–2644. [[CrossRef](#)]
39. Karakaş, M.S.; Günen, A.; Kanca, E.; Yılmaz, C. Boride layer growth kinetics of AISI H13 steel borided with nano-sized powders. *Arch. Metall. Mater.* **2018**, *63*, 159–165.
40. Boonplook, Y.; Juijerm, P. Prediction of Boride Thickness on Tool Steels AISI D2 and AISI H13 Using Boriding Kinetics. *Adv. Mat. Res.* **2014**, *931–932*, 296–300. [[CrossRef](#)]

41. Nait Abdellah, Z.; Boumaali, B.; Keddou, M. Experimental evaluation and modelling the boronizing kinetics of AISI H13 hot work tool steel. *Mater. Test.* **2021**, *63*, 1136–1141. [[CrossRef](#)]
42. Campos, I.; Ramírez, G.; Figueroa, U.; Martínez, J.; Morales, O. Evaluation of boron mobility on the phases FeB, Fe₂B and diffusion zone in AISI 1045 and M2 steels. *App. Surf. Sci.* **2007**, *253*, 3469–3475. [[CrossRef](#)]
43. Hasan, R.; Liew, J.Z.L.; Halim, N. The effect of groove shape on activation energy of powder pack boronizing in mild steel. *J. Tribol.* **2019**, *22*, 123–137.

Disclaimer/Publisher's Note: The statements, opinions and data contained in all publications are solely those of the individual author(s) and contributor(s) and not of MDPI and/or the editor(s). MDPI and/or the editor(s) disclaim responsibility for any injury to people or property resulting from any ideas, methods, instructions or products referred to in the content.